COMPUTER RESEARCH AND MODELING
2026 VOL. 18 NO. 3 P. e621–e641
DOI: 10.20537/2076-7633-2026-18-3-621-641

Ки&М

SPECIAL ISSUE

UDC: 519.8

Physics-informed neural network for evaluating pressure drop in arterial stenoses based on simulation data

T. M. Gamilov[1,a], A. Lange[1,b], A. A. Osipova[1,c], F. Liang[1,2,d], S. S. Simakov[1,3,e]

[1]Sechenov First Moscow State Medical University,
8/2 Trubetskaya st., Moscow, 119048, Russia
[2]Shanghai Jiao Tong University,
800 Dongchuan st., Minhang District, Shanghai, 200240, China
[3]Moscow Institute of Physics and Technology,
9 Institutskii lane, Dolgoprudny, Moscow reg., 141701, Russia

E-mail: [a] gamilov_t_m@staff.sechenov.ru, [b] lange_a@student.sechenov.ru, [c] anastasiia.os1pova@mail.ru,
[d] fuyouliang@sjtu.edu.cn, [e] simakov.ss@phystech.edu

Received 20.03.2026, after completion — 23.04.2026.
Accepted for publication 27.04.2026.

This paper describes a method for generating a synthetic database of stenoses, consisting of 1620 entries. Each entry represents the results of a numerical experiment simulating the three-dimensional flow of a viscous incompressible fluid through a tube with a variable cross-section: pressure drop, mean flow rate, cross-sectionally averaged inlet blood flow velocity, maximum stenosis severity, stenosis length, stenosis asymmetry, tube radius, and Reynolds number. The database was validated by comparison with other models (with elastic walls) and bench experiments, showing a deviation in pressure drops of no more than 4 %. The synthetic stenosis database was used to train a physics-informed neural network for the rapid estimation of pressure drop based on four key input parameters: Reynolds number, stenosis length, stenosis severity, and stenosis asymmetry coefficient. The physics-informed aspect was achieved by introducing penalties into the loss function for the absence of a positive pressure drop and for the lack of monotonicity of the pressure drop with respect to the input parameters. The physics-informed neural network demonstrated higher accuracy on hemodynamically significant stenoses when tested on a validation set and on new stenoses not represented in the database. The mean relative error for stenoses with a length of 8 healthy vessel radii was 6 % for the physics-informed network and 13 % for a classical neural network. The errors for short stenoses with a length of 4 radii were nearly identical: 9.5 % for the physics-informed network and 10 % for the classical neural network. The developed method for the functional assessment of the hemodynamic significance of stenoses can be used both as a standalone tool for clinical stenosis evaluation and as a component of network blood flow models. The approach becomes most relevant when modeling multi-vessel disease, which is predominant in clinical practice. The key advantage of the method lies in the physical correctness of the results and accuracy comparable to classical modeling, but with significantly lower computational costs.

Keywords: physics-informed neural network, synthetic database, stenosis, hemodynamics

Citation: *Computer Research and Modeling*, 2026, vol. 18, no. 3, pp. e621–e641.

КОМПЬЮТЕРНЫЕ ИССЛЕДОВАНИЯ
И МОДЕЛИРОВАНИЕ 2026 Т. 18 № 3 С. e621–e641
DOI: 10.20537/2076-7633-2026-18-3-621-641

Ки&М

СПЕЦИАЛЬНЫЙ ВЫПУСК

УДК: 519.8

Физически информированная нейросеть для оценки перепада давления при артериальных стенозах на основе данных моделирования

Т. М. Гамилов[1,a], А. Ланге[1,b], А. А. Осипова[1,c], Ф. Лян[1,2,d], С. С. Симаков[1,3,e]

[1]Первый МГМУ им. И. М. Сеченова Минздрава России (Сеченовский университет),
Россия, 119048, г. Москва, ул. Трубецкая, д. 8, стр. 2
[2]Шанхайский университет Цзяотун,
Китай, 200240, г. Шанхай, район Миньхан, ул. Дунчуань, 800
[3]Московский физико-технический институт (национальный исследовательский университет, МФТИ, Физтех),
Россия, 141701, Московская область, г. Долгопрудный, Институтский пер., д. 9

E-mail: [a] gamilov_t_m@staff.sechenov.ru, [b] lange_a@student.sechenov.ru, [c] anastasiia.os1pova@mail.ru, [d] fuyouliang@sjtu.edu.cn, [e] simakov.ss@phystech.edu

Получено 20.03.2026, после доработки — 23.04.2026.
Принято к публикации 27.04.2026.

В данной работе описана методика генерации синтетической базы данных стенозов, состоящей из 1620 записей. Каждая запись представляет собой результаты численного эксперимента по моделированию трехмерного течения вязкой несжимаемой жидкости через трубку с переменным сечением: перепад давлений, средний поток, усредненная по сечению скорость кровотока на входе в трубку, максимальная степень сужения стеноза, длина стеноза, асимметрия стеноза, радиус трубки, число Рейнольдса. База данных валидировалась путем сравнения с другими моделями (с эластичными стенками) и стендовыми экспериментами и показала отклонение перепадов давлений не выше 4 %. База данных синтетических стенозов использовалась для обучения физически информированной нейронной сети для быстрой оценки перепада давления по четырем ключевым входным показателям: число Рейнольдса, длина стеноза, степень стеноза, степень асимметрии стеноза. Физическая информированность достигалась за счет введения штрафов в функцию потерь за отсутствие положительного перепада давления и за отсутствие монотонности перепада давления по входным параметрам. Физически информированная нейронная сеть показала более высокую точность на гемодинамических значимых стенозах при тестировании на валидационной выборке и на новых стенозах, не представленных в базе данных. Средняя относительная ошибка на стенозах длиной в 8 радиусов здорового сосуда составила 6 % для физически информированной сети и 13 % для классической нейронной сети. Ошибки на коротких стенозах длиной в 4 радиуса оказались почти одинаковы: 9,5 % для физически информированной сети и 10 % для классической нейронной сети. Разработанный метод функциональной оценки гемодинамической значимости стенозов может использоваться как самостоятельный инструмент для клинической оценки стенозов и как компонент сетевых моделей кровотока. Наибольшую актуальность подход приобретает при моделировании многососудистых поражений, которые доминируют в клинической практике. Ключевое преимущество метода заключается в физической корректности результатов и точности, сопоставимой с классическим моделированием, при значительно меньших вычислительных затратах.

Ключевые слова: физически информированная нейронная сеть, синтетическая база данных, стеноз, гемодинамика

Introduction

Stenosis is a pathological narrowing of an artery that impedes blood flow and hinders the transport of oxygen and nutrients to tissues. Stenoses occur in various segments of the vascular bed. A wide range of methods and tools has been developed for their diagnosis and treatment [Kasapis, Gurm, 2009; Tu et al., 2020; Чернявский и др., 2024]. In recent years, mathematical models of blood flow have been widely used in the development of such methods [El Khatib et al., 2019; Simakov et al., 2021; Gamilov et al., 2024; Xia et al., 2025]. Mathematical models of blood flow make it possible to assess the functional significance of a stenosis, evaluate its effect on different parts of the vascular bed, and predict the outcomes of surgical interventions [Hohri et al., 2024]. At present, software based on numerical modeling of hemodynamics is already used in clinical practice [Boussoussou et al., 2023; Andersen et al., 2024]. The most common mathematical models that provide a detailed description of blood flow in the region of stenoses are three-dimensional models based on the equations of fluid dynamics [Ma et al., 2014; Dobroserdova et al., 2016; Yan et al., 2025]. They can be used either independently or as components of multiscale models. In a multimodel approach [Dobroserdova et al., 2016; Amare et al., 2022; Kim et al., 2026], simple one-dimensional [Gamilov et al., 2015; Буничева и др., 2024] and lumped-parameter zero-dimensional models [El Khatib et al., 2019] are used to analyze most of the circulatory system, whereas three-dimensional models describe the most important and geometrically complex regions, such as stenoses. This approach reduces computational costs and makes it possible to assess the effect of a pathology on blood flow in various parts of the vascular bed.

Another approach to the computational diagnosis of stenoses is machine learning [Danilov et al., 2021; Zimmermann et al., 2021; Ben-Assa et al., 2023; Arefinia et al., 2024]. Machine learning methods have made a significant contribution to the study and diagnosis of cardiovascular diseases. Over many years of clinical practice, a large amount of data has been collected and used for the development of predictive methods. This data includes medical history, patient lifestyle, medical images, etc. Classical machine learning models can be applied to a wide range of tasks; however, they are based on the black-box concept and do not account for the physical laws governing the systems they describe.

Modern approaches combine machine learning techniques with mathematical descriptions of hemodynamic processes. One example of such a synthesis is physics-informed neural networks [Cai et al., 2021; Taebi, 2022; Alzhanov et al., 2024] (PINNs). The architecture or training process of PINNs incorporates physical principles of the process under consideration. Physical principles can be incorporated in several ways.

The first approach is to train a neural network on synthetic data generated with blood flow mathematical models [Bunicheva et al., 2022; Gamilov et al., 2023; Петров, Зимина, 2025]. In this case, the trained neural network reproduces the results of hemodynamic simulations, thereby reducing computational time and resource requirements. The second approach is to modify the loss function so that, during training, the neural network is penalized for nonphysical solutions [Iliadis et al., 2025], for example, for violating the law of mass conservation [Alzhanov et al., 2024; Isaev et al., 2024]. This causes the neural network outputs to satisfy prescribed physical laws or governing equations. The third approach involves the use of specialized activation functions, for example, sinusoidal functions for describing periodic processes [Aghaee, Khan, 2025], or functions arising from analytical solutions of the equations governing the processes under study [Abbasi, Andersen, 2024]. Other ways of incorporating physical information may include modifying the neural network architecture, such as separating individual hidden layers or subnetworks and grouping input data [Liu et al., 2025].

In this paper, we present a physics-informed neural network with a modified loss function for estimating the pressure drop across a stenosis from four input parameters: blood flow velocity, stenosis length, degree of stenosis, and degree of asymmetry, defined as the displacement of the vessel

centerline. The pressure drop is affected by other characteristics, including the vessel cross-sectional shape, vessel curvature, wall stiffness, and pressure sensor position [Ahamad et al., 2018]. The choice of the parameters considered in this study is justified by their significance [Rasooli et al., 2025], feasibility of the problem formulation and available computational resources.

We generate synthetic stenoses database with the help of a three-dimensional model of incompressible fluid flow in a rigid-walled tube with variable cross-section. This database is used to train the neural network. Methods section describes the mathematical model used to generate the synthetic database, the database generation procedure, the neural network architecture, and the modification of the loss function. Results section presents the validation of the database and compares the accuracy of the proposed physics-informed neural network with that of a classical neural network without the modified loss function.

The developed PINN can be used as a standalone tool for assessing the hemodynamic significance of stenoses in clinical practice or as a component of more complex blood flow models. This approach is particularly relevant for modeling blood flow in multivessel arterial disease. Hemodynamically significant atherosclerotic lesions in several vascular beds are most typical in real clinical practice. The advantage of using PINNs for such tasks is that the result is physically consistent and has an accuracy comparable to that of classical numerical modeling, while requiring substantially fewer computational resources.

Methods

Synthetic database of pressure drops across stenoses

To train and test our PINN, a synthetic database was generated, comprised of numerical results of blood flow simulations in stenosed vessels. Numerical simulations were performed using the open-source software package SimVascular [Updegrove et al., 2017; Lan et al., 2018]. This software was chosen because it is specifically designed for computational hemodynamics and provides access to the source code, which ensures the reproducibility of the results.

The mathematical model is based on the Navier – Stokes equations for a three-dimensional flow of a viscous incompressible Newtonian fluid through a cylindrical vessel with a circular cross-section and a stenosis, i. e., a local narrowing. A stationary parabolic velocity profile was prescribed at the inlet. During each simulation we solve an unsteady problem until the flow reached a steady state. Zero pressure was prescribed at the outlet. A no-slip condition was imposed on the vessel walls, which were assumed to be rigid. The equations are written in Cartesian coordinates, with the x-axis aligned with the vessel and connecting the centers of the inlet and outlet cross-sections. The y-axis is aligned with the line of displacement of the cross-section center at the narrowest point

$$\begin{gathered} \rho\left(\frac{\partial \mathbf{u}}{\partial t} + (\mathbf{u}\cdot\nabla)\mathbf{u}\right) = -\nabla p + \mu\nabla^2\mathbf{u}, \\ \nabla\cdot\mathbf{u} = 0, \\ \mathbf{u} = \mathbf{u}_{\text{in}} \text{ on } \Gamma_{\text{in}}, \\ \mathbf{u} = \mathbf{0} \text{ on } \Gamma_w, \end{gathered} \tag{1}$$

where $\mathbf{u}$ is the velocity, $\mathbf{u}_{\text{in}}$ is the inlet velocity, t is time, ρ is the fluid density (ρ = 1.06 g/cm^3), p is pressure, and μ is the dynamic viscosity of the fluid (μ = 0.035 Poise). The boundaries Γ_{in} and Γ_w, corresponding to the vessel inlet and wall, respectively, are shown in Fig. 1. The inlet velocity vector $\mathbf{u}_{\text{in}}$ is normal to the boundary Γ_{in}, and its magnitude is prescribed by a parabolic Poiseuille

profile $u(y, z) = 2\overline{u}\left(1 - \frac{y^2+z^2}{R_0^2}\right)$, where R_0 is the radius of the healthy vessel and $\overline{u}$ is the velocity averaged over Γ_{in}.

At the vessel outlet Γ_{out}, the GenBC condition from SimVascular was used. This condition provides coupling between the three-dimensional computational domain and an analytically prescribed pressure condition [Vignon-Clementel et al., 2006]. The outlet pressure was set to a constant value equal to zero. From the physiological perspective, it makes sense to prescribe a venous pressure or the pressure in small arteries downstream before microcirculation as the outlet pressure. However, numerical experiments show that the value of the outlet pressure does not affect the pressure drop across the stenosis. Therefore, to simplify the problem formulation and comparison with other studies, the outlet pressure was assumed to be zero. The Navier – Stokes equations were solved using the built-in SimVascular functions based on the PHASTA library (Parallel, Hierarchical, Adaptive, Stabilized, Transient Analysis) [Sahni et al., 2009].

The flow regime is characterized by the Reynolds number Re, which in this study is defined using the mean inlet velocity $\overline{u}$:

$$\text{Re} = \frac{\rho \overline{u} D_0}{\mu},$$

where D_0 is the diameter of the nonstenosed part of the vessel (see Fig. 1).

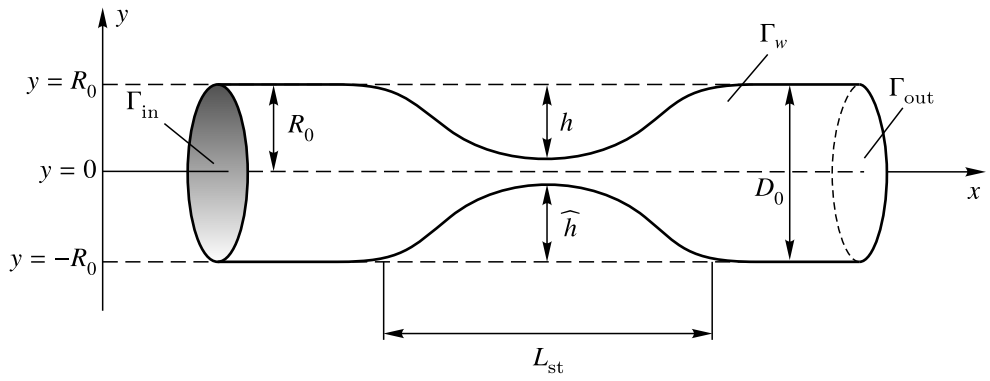

Figure 1. Schematic representation of the computational domain and stenosis parameters

The computational domain is a three-dimensional model of a straight vessel with a local narrowing — stenosis (Fig. 1). In the stenosis region the vessel has a circular cross-section of smaller diameter. The stenosis diameter and radius, D_{st} and R_{st}, are defined as the minimum diameter and radius of the cross-section in the stenosis region. D_0 and R_0 are the diameter and radius of the healthy vessel and L_{st} is the stenosis length. The degree of stenosis λ is defined as

$$\lambda = 1 - \frac{R_{\text{st}}}{R_0}. \tag{2}$$

Stenosis asymmetry has a significant effect on the pressure drop [Vassilevski et al., 2011]. The degree of stenosis asymmetry $\alpha \in [0, 1]$ is defined through the displacement of the center of the circular cross-section along the y-axis relative to the central vessel axis x. The value of α is defined as

$$\alpha = 1 - \frac{h}{R_0 - R_{\text{st}}} = \frac{\widehat{h}}{R_0 - R_{\text{st}}} - 1, \tag{3}$$

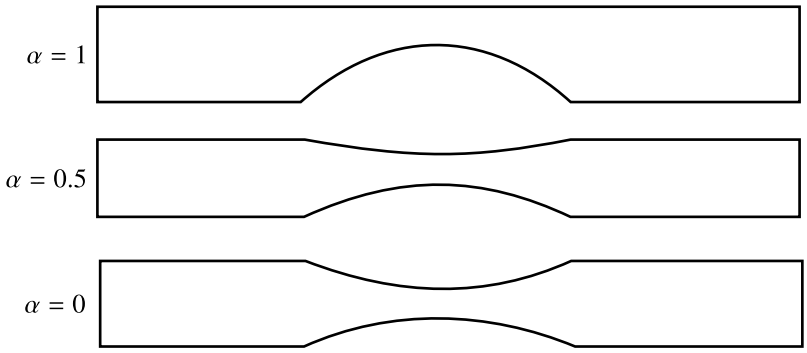

Figure 2. Vessel profiles (in the Oxy plane) for different degrees of asymmetry α

where $\widehat{h}$ is the distance from the lower boundary of the vessel at the narrowest part to the level $y = -R_0$ (see Fig. 1). At $\alpha = 0$, the stenosis is completely symmetric, whereas at $\alpha = 1$ the upper vessel wall in the stenosis region is fully displaced to the level $y = R_0$ (see Fig. 2).

The vessel geometry consists of three regions: a proximal healthy segment corresponding to the inlet part, a stenosis region of length L_{st}, and a distal healthy segment corresponding to the outlet part. The lengths of the proximal and distal segments are fixed and equal to $20R_0$. In all cross-sections perpendicular to the x-axis, the vessel is assumed to be perfectly circular. Therefore, to define the vessel geometry, it is sufficient to specify the function $R(x)$ and, in the presence of asymmetry, the displacement of the cross-section center in the stenosis region. All cross-sections in the stenosis region are displaced in the same direction along the y-axis, which is perpendicular to the x-axis (see Fig. 1).

The vessel radius in the stenosis region is defined as

$$R(x) = R_{\text{st}} + 4(R_0 - R_{\text{st}})\frac{(x - x_c)^2}{L_{\text{st}}^2},$$

where $x \in [20R_0,\ 20R_0 + L_{\text{st}}]$ and $x_c = 20R_0 + \frac{L_{\text{st}}}{2}$. The coordinate $y_c(x)$ of the vessel center in the asymmetric geometry is defined as

$$y_c(x) = \alpha(R_0 - R(x)). \tag{4}$$

When generating the synthetic database, the vessel radius was fixed at $R_0 = 1.5$ mm, which corresponds to a typical radius of major coronary arteries. This value was chosen because the incidence of atherosclerotic lesions in the coronary arteries is among the highest in the systemic circle [Boussoussou et al., 2023; Andersen et al., 2024]. After fixing the vessel radius, the following parameters were varied:

1. Reynolds number Re: 10 values ranging from 30 to 800 which corresponds to a mean velocity $\overline{u}$ from 3 to 89 cm/s in a vessel with a diameter of 3 mm.

2. Ratio of stenosis length to vessel radius $\frac{L_{\text{st}}}{R_0}$: 6 values equal to 2.5, 5, 10, 15, 20, and 30, which at $R_0 = 0.15$ cm correspond to stenosis lengths from 0.375 cm to 4.5 cm.

3. Degree of stenosis λ: 9 values from 0 (healthy vessel) to 0.8 with a step of 0.1.

4. Degree of asymmetry α: $\alpha \in \{0;\ 0.5;\ 1\}$. The value $\alpha = 0$ corresponds to a completely symmetric stenosis, $\alpha = 1$ corresponds to the maximum possible displacement of the stenotic lumen toward the vessel wall (see Fig. 2).

For each combination of parameters, the pressure drop between the beginning and the end of the stenosis was calculated. Taking into account all parameter combinations, the generated database contains 1620 computational cases.

The computational domain was discretized using an unstructured tetrahedral mesh. The mesh density in the healthy vessel region was the same for all cases and was determined by a mesh convergence study performed for a healthy vessel. In this study the number of mesh elements was doubled until the maximum deviation in the calculated pressure became less than 1 %. The mesh density in the stenosis cross-section was multiplied by $\frac{R_0}{R(x)}$, where $R(x)$ is the vessel radius in the corresponding cross-section. Mesh convergence was also selectively verified for vessels with 80 % stenosis by comparing the pressures calculated on successively refined meshes. It was found that the proposed mesh refinement algorithm provides 1 % accuracy during pressure calculations. The resulting number of elements varied from $2.8 \cdot 10^5$ (in the absence of stenosis) to $7.6 \cdot 10^5$ ($L_{\text{st}} = 30R$, $\lambda = 0.8$).

Neural network architecture

In this study, a feed-forward neural network (FFNN) was developed and then modified using the physics-informed neural network (PINN) methodology. The neural network is designed to predict the pressure drop ΔP for prescribed geometric and hemodynamic parameters of a stenosis.

An FFNN is a fully connected feed-forward neural network in which data pass sequentially from the input layer to the output layer without feedback connections. When initializing an FFNN, it is necessary to define the network configuration (the number of layers and neurons) choose the activation functions, specify the loss function and select the optimization algorithm.

Four values are used as inputs to the neural network: the Reynolds number Re, stenosis length L_{st}, degree of stenosis λ and degree of asymmetry α. The neural network output is the predicted value of ΔP.

The following neural network structure is proposed:

- input layer: 4 features, namely Re, stenosis length L_{st}, degree of stenosis λ, and asymmetry α;
- two hidden layers with 16 neurons in each layer;
- activation function of the hidden layers: hyperbolic tangent [Goodfellow et al., 2016]. This function ensures smoothness of the output function, which is critical for calculating derivatives in the physical part of the loss function;
- output layer consisting of one neuron: the pressure drop across the stenosis.

The target variable in the output layer, ΔP, was first transformed using the function $\log(1 + \Delta P)$ and then normalized with respect to the minimum and maximum values using PyTorch MinMaxScaler. The logarithmic transformation of the pressure drop was used to reduce the range of absolute values. All input features were also normalized with respect to their minimum and maximum values. Let Y denote the transformed and normalized value of the target variable ΔP, and let X_{Re}, $X_{L_{\text{st}}}$, X_{λ}, X_{α} denote the normalized values of the features Re, L_{st}, λ, α.

The neural network architecture was the same for FFNN and PINN because the main goal was to compare the standard FFNN with its physics-informed extension. The number of layers, the width of the hidden layers, the type of activation function, and the learning rate were selected based on preliminary trial experiments.

The loss function must be nonnegative, continuous, and differentiable, which ensures interpretability of the error and makes it possible to apply gradient-based methods. In this study, the classical MSE and a loss function with physical regularization are used.

The mean squared error (MSE) is defined as

$$\mathrm{MSE} = \frac{1}{2N}\sum_{i=1}^{N}(Y_i - \widehat{Y}_i)^2, \tag{5}$$

where N is the number of elements in the training sample, Y_i are the normalized pressure drop values from the synthetic database for i-th stenosis, and $\widehat{Y}_i$ are the normalized pressure drop values predicted by the neural network for i-th stenosis.

For the PINN modification of the FFNN the following constraints are imposed during training to improve the physical consistency of the relationship between the inputs and the output: penalties for deviations from monotonicity of the pressure drop with respect to the input parameters and a penalty for a negative pressure drop in the downstream direction. These constraints are derived from the following considerations. The pressure drop across a vascular segment with a stenosis characterizes the energy losses of the blood flow. Its monotonic dependence on the input geometric and hemodynamic parameters is determined by the mechanisms of energy dissipation.

An increase in stenosis length leads to an increase in hydrodynamic resistance, because the length of the region in which viscous blood experiences friction against the immobile vessel wall increases. The longer the narrowed segment, the more energy is lost due to friction forces. This causes an additional pressure gradient to maintain a constant flow rate.

The degree of narrowing affects the pressure drop due to the flow continuity law. As the lumen cross-section decreases, the blood velocity in the stenosis increases. This leads, first, to an increase in the kinetic energy required to accelerate the fluid and, second, to an increase in shear stresses and viscous friction, which further increases the losses.

The role of the Reynolds number is manifested in changes in the flow structure and in the ratio between different loss mechanisms. As Re increases, energy losses associated with vortex formation in the post-stenotic region increase, making the dependence of the pressure drop on blood flow rate steeper; however, the overall character of this dependence remains monotonically increasing.

The displacement of the stenotic lumen center relative to the longitudinal vessel axis increases hydrodynamic resistance due to the disruption of flow symmetry. In an asymmetric narrowing, the velocity profile is deformed, and an extensive flow separation zone appears on the side opposite to the displacement of the lumen center. The formation of vortical structures downstream of the stenosis requires additional mechanical energy expenditure, which leads to a monotonic increase in the pressure drop across the stenosis as the degree of displacement of the lumen center from the axial line increases.

The monotonically nondecreasing dependence of the predicted pressure drop on the input parameters is proposed to be represented as

$$\frac{\partial\widehat{Y}}{\partial X_{\mathrm{Re}}} \geqslant 0, \quad \frac{\partial\widehat{Y}}{\partial X_{L_{\mathrm{st}}}} \geqslant 0, \quad \frac{\partial\widehat{Y}}{\partial X_{\lambda}} \geqslant 0, \quad \frac{\partial\widehat{Y}}{\partial X_{\alpha}} \geqslant 0. \tag{6}$$

This reflects the following considerations: as the Reynolds number, stenosis length, degree of lumen narrowing, and its asymmetry increase, the energy losses associated with flow resistance increase, and therefore the pressure drop must also increase. These considerations are consistent with experimental and mathematical modeling studies [Young, Tsai, 1973; Ma et al., 2014; El Khatib et al., 2019; Ventre et al., 2019; Alzhanov et al., 2024; Gamilov et al., 2024; Xia et al., 2025]. The derivatives with respect to the input parameters were calculated using automatic differentiation, as described, for example, in [Baydin et al., 2018; Raissi et al., 2019; Конюхов и др., 2024].

To include the constraints (6) in the loss function, a penalty for monotonicity violation is introduced. It is calculated as the mean over the training sample of the sum of partial penalties, where each partial penalty is the square of the negative part of the corresponding partial derivative:

$$\mathrm{Loss}_{\mathrm{mono}} = \frac{1}{N}\sum_{i=1}^{N}\left(E^i_{\mathrm{Re}} + E^i_{L_{\mathrm{st}}} + E^i_{\lambda} + E^i_{\alpha}\right), \tag{7}$$

where N is the number of objects in the training sample, and E^i_{Re}, $E^i_{L_{\mathrm{st}}}$, E^i_{λ}, and E^i_{α} are the penalties for the i-th stenosis in the training sample for violations of monotonicity with respect to the corresponding parameter. Each of the penalties is calculated as

$$E^i_{\phi} = \theta(\xi_{\phi})\xi^2_{\phi}, \tag{8}$$

where $\theta(\xi)$ is the Heaviside function, $\xi_{\phi} = -\frac{\partial\widehat{Y}}{\partial X_{\phi}}$, and ϕ is a symbolic variable, $\phi \in \{\mathrm{Re}, L_{\mathrm{st}}, \lambda, \alpha\}$.

The second physical constraint is that the predicted pressure drop, represented by the variable $\widehat{Y}$, must be nonnegative:

$$\widehat{Y} \geqslant 0. \tag{9}$$

The corresponding penalty is

$$\mathrm{Loss}_{\mathrm{neg}} = \frac{1}{N}\sum_{i=1}^{N} E^i_{\mathrm{neg}}, \tag{10}$$

$$E^i_{\mathrm{neg}} = \theta(-\widehat{Y}_i)\widehat{Y}^2_i. \tag{11}$$

The physics-informed loss function takes the form

$$\mathrm{PhysLoss} = \frac{1}{N}\sum_{i=1}^{N}\left(E^i_{\mathrm{Re}} + E^i_{L_{\mathrm{st}}} + E^i_{\lambda} + E^i_{\alpha} + E^i_{\mathrm{neg}}\right). \tag{12}$$

Thus, the total loss function is

$$\mathrm{TotalLoss} = \mathrm{MSE} + \omega\mathrm{PhysLoss}, \tag{13}$$

where ω is a weight coefficient. We use $\omega = 10^{-3}$ because at this value the contributions of the physics-informed and main parts of the loss function are comparable in magnitude.

The neural network was trained using the Adam optimizer with a learning rate of 10^{-4} for $3 \cdot 10^4$ epochs. For the PINN full-batch training was used; the physical part of the loss function was calculated simultaneously over all points in the training sample. This ensures correct calculation of the derivatives and stability of the physical penalty. This approach is consistent with the classical implementation of PINNs [Raissi et al., 2019].

The original dataset was divided into training and validation samples in an 80 % to 20 % ratio, respectively. The split was performed randomly with a uniform distribution. The validation sample was used to analyze the degree of overfitting and to optimize the neural networks, including hyperparameter tuning and modification of the network architecture.

To compare the FFNN and the PINN, a test sample was used. It included a set of separately generated stenosis models that were not included in the synthetic database. The test sample makes it possible to assess the ability of the neural network to generalize results to new cases that were not

present in the training sample. The test sample included stenoses with length-to-radius ratios $\frac{L_{st}}{R_0}$ equal to 8 and 4, and degrees of stenosis of 33 % and 66 %. For each combination of stenosis length and degree of stenosis in the test sample, stenoses were generated for all Reynolds numbers (10 values) and all degrees of asymmetry (3 values). Thus, the test sample includes $2 \cdot 2 \cdot 10 \cdot 3 = 120$ samples.

The derivatives in (7) and (8) were calculated using the same scaled input data as those used by the neural network. Since the physical penalty is based on normalized gradients, scaling does not affect the correctness of the calculations.

The following metrics were used to evaluate and compare the standard FFNN with the PINN.

1. R^2 is the coefficient of determination, i. e., the proportion of the variance of the true values explained by the prediction model:

$$R^2 = 1 - \frac{\sum\limits_{i=1}^{N}(\Delta P_i - \Delta\widehat{P}_i)^2}{\sum\limits_{i=1}^{N}(\Delta P_i - \overline{\Delta P})^2}, \tag{14}$$

   where $\overline{\Delta P} = \frac{1}{N}\sum\limits_{i=1}^{N}\Delta P_i$ is the mean pressure drop.

2. WAPE is the weighted absolute percentage error, i. e., the mean absolute error normalized by the sum of the absolute true values. This parameter shows the average relative error of the prediction model, expressed as a percentage:

$$\mathrm{WAPE} = \frac{\sum\limits_{i=1}^{N}|\Delta P_i - \Delta\widehat{P}_i|}{\sum\limits_{i=1}^{N}|\Delta P_i|}100\,\%. \tag{15}$$

3. sMAPE is the symmetric mean absolute percentage error, i. e., the error normalized by the sum of the absolute values of the true and predicted values. This parameter is less sensitive to small values of the target variable:

$$\mathrm{sMAPE} = \frac{100\,\%}{N}\sum_{i=1}^{N}\frac{2|\Delta P_i - \Delta\widehat{P}_i|}{|\Delta P_i| + |\Delta\widehat{P}_i|}. \tag{16}$$

4. $\frac{\mathrm{MAE}}{\sigma}$ is the mean absolute error divided by the standard deviation of the true values. This parameter shows the ratio of the typical model error to the error associated with the natural variability of the data:

$$\mathrm{MAE} = \frac{1}{N}\sum_{i=1}^{N}|\Delta P_i - \Delta\widehat{P}_i|, \tag{17}$$

$$\sigma = \sqrt{\frac{1}{N}\sum_{i=1}^{N}(\Delta P_i - \Delta\widehat{P}_i)^2}. \tag{18}$$

Results

Validation of the synthetic database

The proposed numerical model was validated by comparing the obtained results with two independent sources: results obtained from blood flow simulations in simplified symmetric models [Ventre et al., 2019] and in vitro experimental data [Young, Tsai, 1973].

In the first series of numerical validation experiments, the Multi-Ring model [Ventre et al., 2019] was used as the reference model. The Multi-Ring model is a numerical method developed for solving the Navier – Stokes equations in an axisymmetric formulation, that is, as two-dimensional equations in cylindrical coordinates. It accounts for wall elasticity and wall motion by coupling the numerical solution with a wall deformation law. This model was used to assess the effect of wall compliance on the pressure drop. In [Ventre et al., 2019], the high accuracy of the Multi-Ring model in calculating the pressure drop across axisymmetric stenoses was demonstrated by comparison with other models and in vivo measurements.

In the first series of numerical experiments, the pressure drop in a vessel with an axisymmetric stenosis was calculated. The boundary conditions were analogous to the formulation (1). The vessel geometry was taken in accordance with the description in [Ventre et al., 2019]. The SimVascular results for axisymmetric stenoses are in close agreement with the Multi-Ring results over a wide range of narrowing degrees (Fig. 3). The mean deviation of the SimVascular numerical experiment from the Multi-Ring model was 2.17 %. The normalized pressure profile along the vessel axis obtained in SimVascular is also identical to the profiles predicted by the Multi-Ring model (Fig. 4).

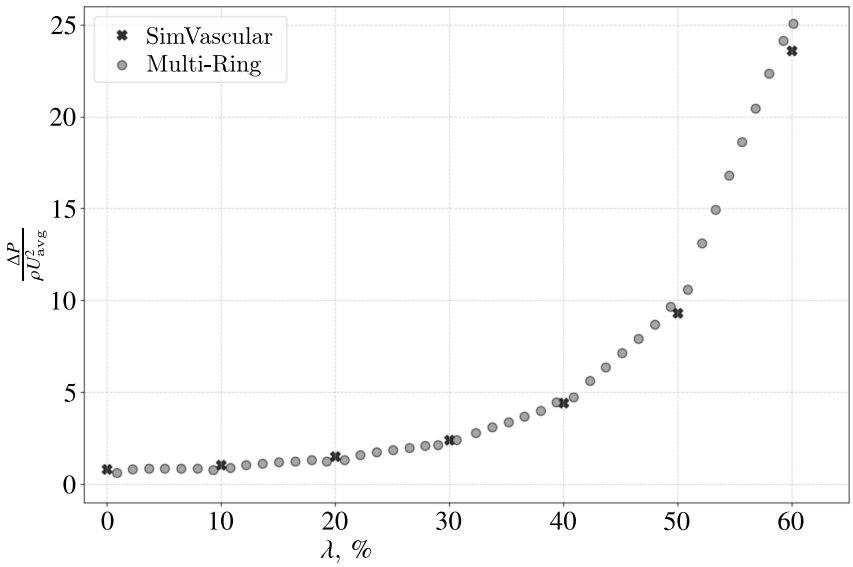

Figure 3. Dimensionless pressure drop in the vessel as a function of the degree of stenosis for the Multi-Ring model [Ventre et al., 2019] and formulation (1) implemented in SimVascular

In the axisymmetric formulation and under laminar flow conditions, the Multi-Ring model is equivalent to a three-dimensional fluid flow model [Ventre et al., 2019]; however, the Multi-Ring model also accounts for vessel wall elasticity. Since the Multi-Ring results are in close agreement with the SimVascular calculations performed with rigid walls, it can be concluded that accounting for wall elasticity does not make a substantial contribution to the prediction of the pressure drop for the stenoses considered. Thus, the rigid-wall model demonstrates sufficient accuracy for pressure drops in steady flow.

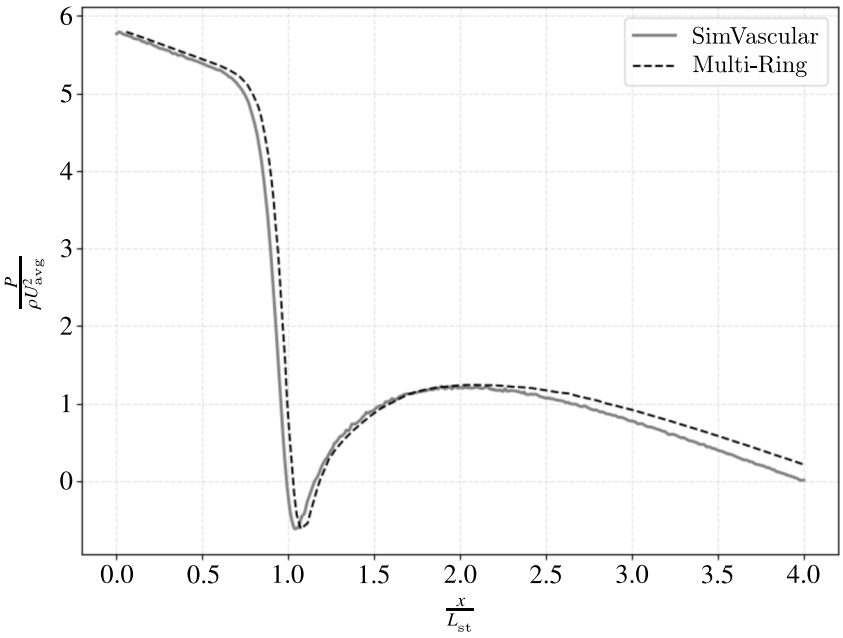

Figure 4. Dimensionless pressure along the vessel for stenosis $\lambda = 0.4$ for the Multi-Ring model [Ventre et al., 2019] and formulation (1) implemented in SimVascular

In the second series of validation experiments, the simulation results were compared with classical in vitro experiments for asymmetric stenoses reported in [Young, Tsai, 1973].

The results in [Young, Tsai, 1973] were obtained in a series of hydrodynamic experiments using distilled water (assumed to be a Newtonian fluid) as the working fluid in physical models of arterial stenoses. The main distinguishing feature of these experiments is the use of asymmetric stenoses. For validation, an asymmetric stenosis, model M-5 from [Young, Tsai, 1973], with a degree of stenosis $\lambda = 0.67$ and $L_{\text{st}} = 8R_0$, was used. The vessel geometry was reproduced exactly in the SimVascular simulations. In this experiment, the pressure drop between the beginning of the vessel and points located along the vessel axis was calculated.

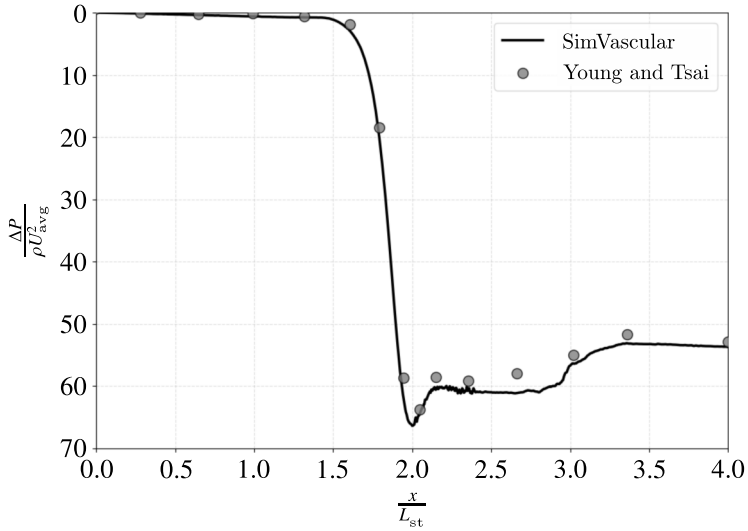

Figure 5. Dimensionless pressure drop along the vessel for an asymmetric stenosis at Re = 900. SimVascular: results obtained using formulation (1); Young and Tsai: laboratory experiment results [Young, Tsai, 1973]

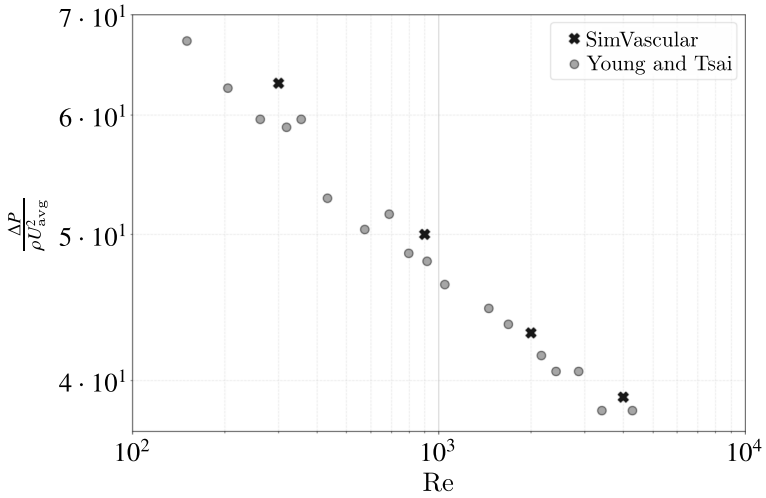

Figure 6. Dimensionless pressure drop across an asymmetric stenosis (α = 0.5) at different Reynolds numbers. SimVascular: results obtained using formulation (1); Young and Tsai: laboratory experiment results [Young, Tsai, 1973]. The axes are shown on a logarithmic scale

The comparison showed good quantitative agreement between the SimVascular results and the experimental data from [Young, Tsai, 1973], both for the pressure drop along the vessel axis (Fig. 5) and for the dependence of the total pressure drop on the Reynolds number (Fig. 6). The mean deviation of the SimVascular numerical experiment from the in vitro experiment was 3.55 %.

The obtained results confirm that the problem formulation and numerical experiment used in SimVascular are correct and applicable for calculating the pressure drop in both axisymmetric and complex asymmetric geometries.

To generate the synthetic database covering the parameter range described in this study 1620 simulations were performed. The simulations were carried out using the high-performance computing cluster of the Institute of Computer Science and Mathematical Modeling of Sechenov University.

Estimation of pressure drops using the neural network

This section presents a comparative analysis of the accuracy of pressure drop estimation using the FFNN and the PINN. First, we evaluate how the introduction of physically justified regularization terms affects the stability of neural network modeling and assess the difference between the FFNN and the PINN on the validation sample.

Both neural networks were trained using the same initial weights and the same hyperparameters for $3 \cdot 10^4$ epochs. Figure 7 shows the training curves of the FFNN and the PINN $1.4 \cdot 10^4$ epochs. After $1.4 \cdot 10^4$ epochs, the training error of both neural networks is certainly below 1 %. Therefore, this interval is considered sufficiently long for a correct comparison. Figure 7 also shows that the FFNN error decreases faster and that the FFNN demonstrates smoother error curves. The PINN trains more slowly and has less smooth transient regions because the physical constraints make the optimization problem more complex. However, it is precisely because of these constraints that the PINN finds more stable and physically consistent solutions outside the training sample. No overfitting is observed from the obtained learning curves: the values on the training and validation samples are almost identical for both neural networks across all metrics. This means that, after each weight update, the model quality was evaluated on data that were not used in training, and the neural network showed comparable results.

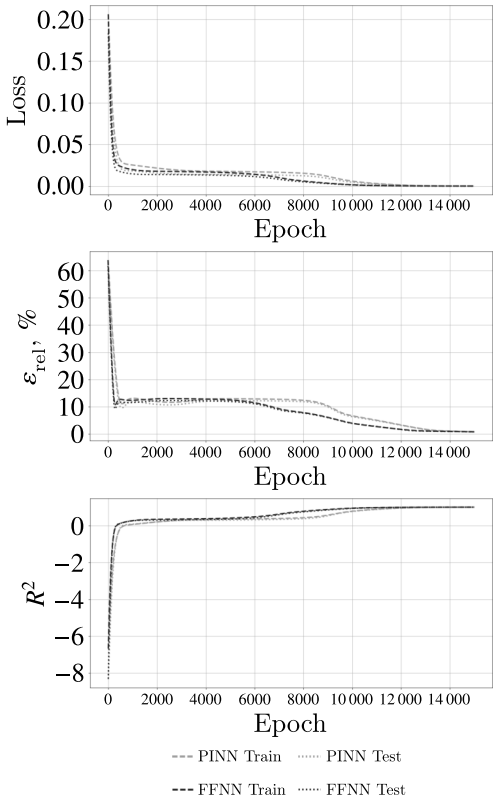

Figure 7. Comparison of the FFNN and PINN learning curves

Figure 8 shows that both neural networks demonstrate high accuracy on the validation set; however, in the region of large pressure drops, the PINN points are closer to the line corresponding to perfect agreement.

In the next series of numerical experiments, the accuracy of pressure drop prediction was studied on a test set consisting of stenoses that were not included in the synthetic database (Fig. 9). For the PINN, the median errors on the test sample are 2–9 %, whereas for the FFNN this range is 8–30 %, indicating the higher stability and accuracy of the PINN.

Table 1 presents the final comparison results for the PINN and the FFNN. The first four rows show the results obtained on the validation set. The validation set consists of 20 % of the records (stenoses) from the database and includes 324 cases with degrees of stenosis from 0 % to 80 %, Reynolds numbers from 30 to 800, stenosis lengths from 2.5 to 30 vessel radii, and three degrees of asymmetry, namely, 0, 0.5, and 1. The last two rows show the mean relative errors (MRE) on the testing set. The testing set consists of records, i. e., stenoses, not represented in the database and includes 120 cases with degrees of stenosis of 33 % and 66 %, Reynolds numbers from 30 to 800, stenosis lengths of 4 and 8 vessel radii, and three degrees of asymmetry, namely, 0, 0.5, and 1.

Based on the data presented in Table 1, the PINN systematically outperforms the FFNN across all metrics. The PINN has a higher R^2, whereas WAPE, sMAPE, and the normalized error $\frac{\text{MAE}}{\sigma}$ are lower. The advantage is especially noticeable on the testing set: the MRE for new stenosis configurations lies in the range of 2.3–12.9 % for the PINN, whereas for the FFNN this range is 6–30 %.

Overall, the PINN outperformed the neural network with the classical architecture. It provides lower errors and operates more stably for stenoses with new sets of input values.

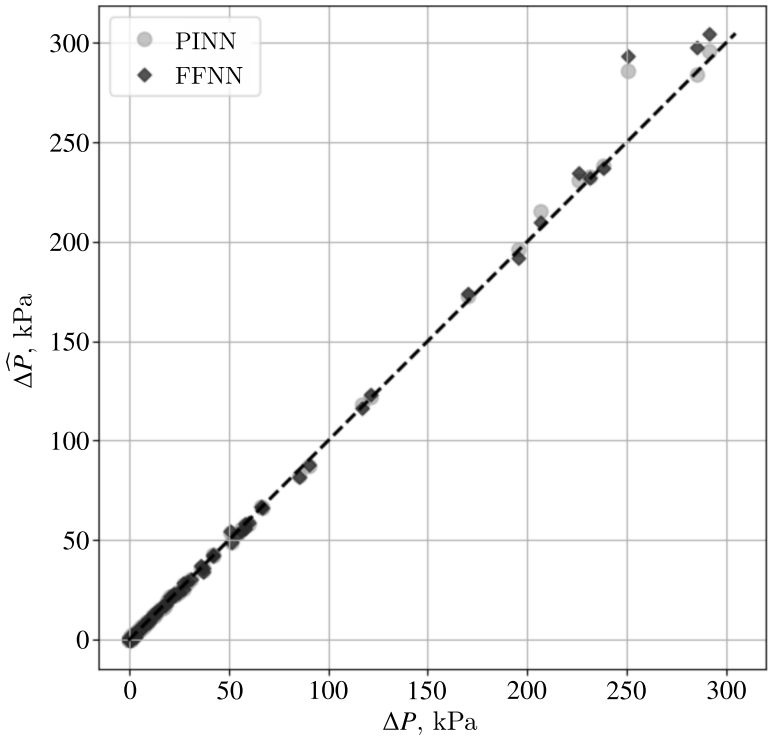

Figure 8. Comparison of the true values, computed from numerical simulations, and the predicted values of the pressure drop ΔP for the FFNN and the PINN on the validation set. The validation set is comprised of cases from the synthetic database with degrees of stenosis from 0 % to 80 %

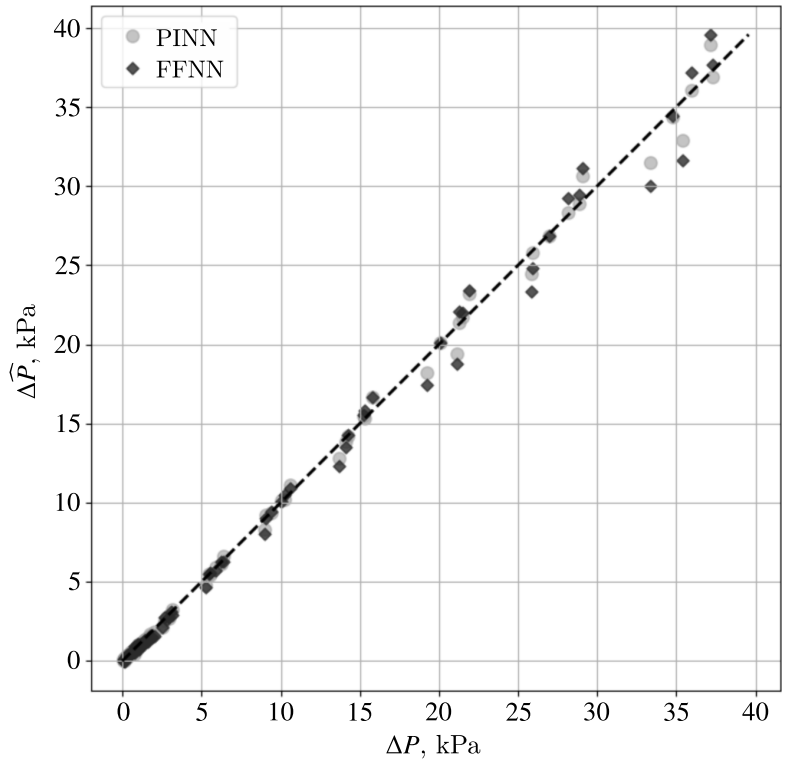

Figure 9. Comparison of the true and predicted values of the pressure drop ΔP for the PINN and the FFNN on the testing set. The testing set is comprised of 120 separately generated stenoses with degrees of stenosis of 33 % and 66 %

Table 1. Comparison of the accuracy of the PINN and the FFNN

Metric	PINN	FFNN
R^2	0.9973	0.9956
WAPE	2.97 %	4.36 %
sMAPE	33.76 %	44.52 %
$\frac{\text{MAE}}{\sigma}$	0.91 %	1.34 %
MRE ($L_{st} = 4R_0$)	6.22 %	13.31 %
MRE ($L_{st} = 8R_0$)	9.45 %	9.90 %

Discussion

There are two main approaches to predicting the pressure drop across stenoses: computational fluid dynamics (CFD) and machine learning (ML) methods. Classical CFD provides high accuracy but requires substantial computational resources and time. Reduced-order models are used to decrease simulation time; however, they have limited accuracy for complex spatial configurations and high Re. Classical machine learning methods do not account for physical laws and require large training datasets. The collection of such datasets is time-consuming and resource-intensive and requires the involvement of a large number of highly qualified experts.

In this study, we proposed a method for estimating the pressure drop across a stenosis that combines mathematical modeling and machine learning approaches. To train the neural network, a synthetic database consisting of 1620 stenoses was generated. The database was generated using a model of viscous incompressible fluid flow through a rigid-walled tube with variable cross-section. The correctness of the simulation results is supported by comparison with the results of other numerical experiments (Figs. 3, 4), including those accounting for arterial wall elasticity, as well as with the results of in vitro experiments (Figs. 5, 6). The calculated pressure profiles are consistent with the experimental data for different flow regimes, with deviations not exceeding 3–4 %.

The generated database was used to train the PINN. The pressure drops predicted by the neural network are consistent with the pressure drops calculated using mathematical modeling (Figs. 8, 9, Table 1). At the same time, the PINN demonstrates an error that is 1.5–2 times lower than that of the FFNN. This difference is especially pronounced when predicting pressure drops for stenoses that were not included in the database and have a length of 8 vessel radii (Table 1). This indicates the ability of the PINN to generalize the results to new cases and its lower dependence on the size and density of the training sample.

Compared with other PINNs developed for assessing the hemodynamic significance of stenoses [Zhang et al., 2023; Alzhanov et al., 2024], the present study does not use data from real patients, and the vessel geometries are simplified. Only four parameters are provided as inputs to the neural network. This makes the generated database less accurate but more universal and easier to use. The developed neural network and database can be used to estimate pressure drops across stenoses in different parts of the vascular bed, including coronary vessels, carotid arteries, and femoral arteries. In addition, the simplicity of the input dataset facilitates the integration of the neural network into other blood flow models. On the other hand, further development of the proposed approach requires validation using real patient data and expansion of the set of parameters describing the geometry and other characteristics of stenoses.

One important result is the improved accuracy of the PINN compared with the standard neural network, especially for “new” stenoses that were not present in the training sample. It is interesting to note that the improvement in accuracy is minor for short stenoses (Table 1, stenoses of length $4R_0$), but more pronounced for long stenoses (Table 1, stenoses of length $8R_0$).

One limitation of this study is the use of a vessel with a fixed radius of 1.5 mm to generate the entire database. This limitation can be addressed using hydrodynamic similarity. For a vessel of another diameter, one can calculate the dimensionless ratios of stenosis length to diameter, the Reynolds number, the degree of stenosis, and the degree of asymmetry, and then reduce the problem to the case of a stenosis in a vessel with a radius of 1.5 mm. To overcome this limitation, future work will include testing the use of the database for stenoses of different diameters, as well as investigating the possibility of extending the database without performing additional simulations by nondimensionalizing the problem formulation.

Conclusion

This study describes a method for generating a synthetic database of stenoses consisting of 1620 records. The database was validated by comparison with other models, including models with elastic walls, and with bench-top experiments, demonstrating deviations in pressure drops not exceeding 4 %.

The synthetic stenosis database was used to train a PINN for rapid estimation of the pressure drop from four key parameters: Reynolds number, stenosis length, degree of stenosis, and degree of stenosis asymmetry. The PINN showed higher accuracy for hemodynamically significant stenoses when tested on the validation and test samples. The mean relative error for stenoses with a length of 8 healthy-vessel radii was 6 % for the physics-informed neural network and 13 % for the classical neural network. For short stenoses with a length of 4 radii, the errors were almost identical: 9.5 % for the PINN and 10 % for the FFNN.

In future work, the database is planned to be expanded by including critical stenoses with diameter narrowing up to 90 % and by increasing the number of varied stenosis characteristics that affect the pressure drop, including stenosis profile shape, vessel curvature, and different types of stenosis asymmetry [Rasooli et al., 2025]. Further validation of the neural network using real patient data is also planned, as well as its integration into a one-dimensional network model of blood flow [Gamilov et al., 2024].

The method for functional assessment of the hemodynamic significance of stenoses developed in this study, namely, the PINN-based approach, is a universal tool that can be integrated into clinical practice and scientific research in several directions. First of all, the method can be used independently for noninvasive assessment of the effect of stenoses on blood flow parameters, which is of high diagnostic value in itself. At the same time, the principles underlying the PINN make it possible to use it as a basic component in the construction of more complex hemodynamic models, thereby expanding the possibilities for comprehensive analysis of vascular pathology.

The potential application of this approach to modeling blood flow under conditions of multivessel arterial disease deserves particular attention. As clinical practice shows, the combination of hemodynamically significant stenoses in several vascular beds of one or different organs is the most common scenario in cardiovascular disease progression. In this context the developed method becomes especially important, since it makes it possible to adequately represent complex interactions between multiple lesion sites.

The principal advantage of the proposed approach is the optimal balance between the physical reliability of the results and computational efficiency. The data obtained using the PINN are physically consistent and demonstrate an accuracy comparable to that of classical hemodynamic modeling. At the same time, a substantial reduction in computational cost is achieved, which opens up opportunities for a wide implementation of the method both in research practice and in clinical applications, where rapid result generation and the ability to process large amounts of data are critically important.

References

Буничева А. Я., Мухин С. И., Соснин Н. В., Хруленко А. Б. Квазиодномерные модели гемодинамики // Вестник Московского университета. Сер. 15. Вычислительная математика и кибернетика. — 2024. — № 4. — С. 44–59.

Bunicheva A. Ya., Mukhin S. I., Sosnin N. V., Khrulenko A. B. Kvaziodnomernye modeli gemodinamiki [Quasi-one-dimensional hemodynamic models] // Moscow University Computational Mathematics and Cybernetics. — 2024. — No. 4. — P. 44–59 (in Russian).

Конюхов И. В., Конюхов В. М., Черница А. А., Дюсенова А. Особенности применения физически информированных нейронных сетей для решения обыкновенных дифференциальных уравнений // Компьютерные исследования и моделирование. — 2024. — Т. 16, № 7. — С. 1621–1636.

Konyukhov I. V., Konyukhov V. M., Chernitsa A. A., Dyussenova A. Osobennosti primeneniya fizicheski informirovannykh neironnykh setey dlya resheniya obyknovennykh differentsial'nykh uravneniy [Analysis of the physics-informed neural network approach to solving ordinary differential equations] // Computer Research and Modeling. — 2024. — Vol. 16, No. 7. — P. 1621–1636 (in Russian).

Петров М. Н., Зимина С. В. Суррогатный нейросетевой метод восстановления поля течения из однородного поля итерациями в расчетах стационарных турбулентных течений // Компьютерные исследования и моделирование. — 2025. — Т. 17, № 2. — С. 179–197.

Petrov M. N., Zimina S. V. Surrogatnyy neyrosetevoy metod vosstanovleniya polya techeniya iz odnorodnogo polya iteratsiyami v raschetakh statsionarnykh turbulentnykh techeniy [A surrogate neural network method for restoring the flow field from a homogeneous field by iterations in calculations of steady turbulent flows] // Computer Research and Modeling. — 2025. — Vol. 17, No. 2. — P. 179–197 (in Russian).

Чернявский М. А., Иртюга О. Б., Янишевский С. Н., Алиева А. С., Самочерных К. А., Абрамов К. Б., Вавилова Т. В., Лукьянчиков В. А., Курапеев Д. И., Ванюркин А. Г., Чернова Д. В., Шелуханов Н. К., Козленок А. В., Кавтеладзе З. А., Малеванный М. В., Виноградов Р. А., Хафизов Т. Н., Иванова Г. Е., Жуковская Н. В., Фокин А. А., Игнатьев И. М., Карпенко А. А., Игнатенко П. В., Астапов Д. А., Семенов В. Ю., Порханов В. А., Крылов В. В., Усачев Д. Ю., Светликов А. В., Алекян Б. Г., Акчурин Р. С., Чернявский А. М., Конради А. О., Шляхто Е. В. Российский консенсус по диагностике и лечению пациентов со стенозом сонных артерий // Российский кардиологический журнал. — 2024. — Т. 27, № 11. — 5284.

Chernyavsky M. A., Irtyuga O. B., Yanishevsky S. N., Alieva A. S., Samochernykh K. A., Abramov K. B., Vavilova T. V., Lukyanchikov V. A., Kurapeev D. I., Vanyurkin A. G., Chernova D. V., Shelukhanov N. K., Kozlyonok A. V., Kavteladze Z. A., Malevanny M. V., Vinogradov R. A., Khafizov T. N., Ivanova G. E., Zhukovskaya N. V., Fokin A. A., Ignatiev I. M., Karpenko A. A., Ignatenko P. V., Astapov D. A., Semenov V. Yu., Porkhanov V. A., Krylov V. V., Usachev D. Yu., Svetlikov A. V., Alekyan B. G., Akchurin R. S., Chernyavsky A. M., Konradi A. O., Shlyakhto E. V. Rossiiskii konsensus po diagnostike i lecheniyu patsientov so stenozom sonnykh arterii [Russian consensus statement on the diagnosis and treatment of patients with carotid stenosis] // Russian Journal of Cardiology. — 2024. — Vol. 27, No. 11. — 5284 (in Russian).

Abbasi J., Andersen P. O. Physical activation functions (PAFs): An approach for more efficient induction of physics into physics-informed neural networks (PINNs) // Neurocomputing. — 2024. — Vol. 608. — 128352.

Aghaee A., Khan M. O. Pinning down the accuracy of physics-informed neural networks under laminar and turbulent-like aortic blood flow conditions // Comput. Biol. Med. — 2025. — Vol. 185. — 109528.

Ahamad N. A., Kamangar S., Badruddin I. A. The influence of curvature wall on the blood flow in stenosed artery: A computational study // Biomedical Materials Engineering. — 2018. — Vol. 29, No. 3. — P. 319–332.

Alzhanov N., Ng E. Y. K., Zhao Y. Three-dimensional physics-informed neural network simulation in coronary artery trees // Fluids. — 2024. — Vol. 9, No. 7. — 153.

Amare R., Hodneland E., Roberts J. A., Bahadori A. A., Eckels S. Modeling a 3-D multiscale blood-flow and heat-transfer framework for realistic vascular systems // Sci. Rep. — 2022. — Vol. 12, No. 1. — 14610.

Andersen B. K., Sejr-Hansen M., Maillard L., Campo G., Råmunddal T., Stähli B. E., Guiducci V., Serafino L. D., Escaned J., Santos I. A., López-Palop R., Landmesser U., Dieu R. S., Mejía-Rentería H., Koltowski L., Žiubrytė G., Cetran L., Adjedj J., Abdelwahed Y. S., Liu T., Mogensen L. J. H., Eftekhari A., Westra J., Lenk K., Casella G., Van Belle E., Biscaglia S., Olsen N. T., Knaapen P., Kochman J., Santos R. C., Scarsini R., Christiansen E. H., Holm N. R. Quantitative flow ratio versus fractional flow reserve for coronary revascularisation guidance (FAVOR III Europe): a multicentre, randomised, non-inferiority trial // The Lancet — 2024. — Vol. 404, No. 10465. — P. 1835–1846.

Arefinia F., Aria M., Rabiei R., Hosseini A., Ghaemian A., Roshanpoor A. Non-invasive fractional flow reserve estimation using deep learning on intermediate left anterior descending coronary artery lesion angiography images // Sci. Rep. — 2024. — Vol. 14. — 1818.

Baydin A. G., Pearlmutter B. A., Radul A. A., Siskind J. Automatic differentiation in machine learning: A survey // J. Mach. Learn. Res. — 2018. — Vol. 18, No. 153. — P. 1–43.

Ben-Assa E., Abu Salman A., Cafri C., Roguin A., Hellou E., Koifman E., Feld Y., Lev E., Sheinman G., Harari E., Abu Dogosh A., Beyar R., Garcia-Garcia H. M., Davies J., Ben-Yehuda O. Performance of a novel artificial intelligence software developed to derive coronary fractional flow reserve values from diagnostic angiogram // Coron. Artery Dis. — 2023. — Vol. 34, No. 8. — P. 533–541.

Boussoussou M., Édes I. F., Nowotta F., Vattay B., Vecsey-Nagy M., Drobni Z., Simon J., Kolossváry M., Németh B., Jermendy Á. L., Becker D., Leipsic J., Rogers C., Collinsworth A., Maurovich-Horvat P., Merkely B., Szilveszter B. Coronary CT-based FFR in patients with acute myocardial infarction might predict follow-up invasive FFR: The XPECT-MI study // J. Cardiovasc. Comput. Tomogr. — 2023. — Vol. 17, No. 4. — P. 269–276.

Bunicheva A. Y., Kochetov E. V., Mukhin S. I. Mathematical model of building a neural network for diagnosing circulatory disorders // Moscow Univ. Comput. Math. Cybern. — 2022. — Vol. 46. — P. 125–132.

Cai S., Mao Z., Wang Z., Yin M., Karniadakis G. E. Physics-informed neural networks (PINNs) for fluid mechanics: a review // Acta Mech. Sin. — 2021. — Vol. 37. — P. 1727–1738.

Danilov V. V., Klyshnikov K. Yu., Gerget O. M., Kutikhin A. G., Ganyukov V. I., Frangi A. F., Ovcharenko E. A. Real-time coronary artery stenosis detection based on modern neural networks // Sci. Rep. — 2021. — Vol. 11, No. 1. — 7582.

Dobroserdova T., Olshanskii M., Simakov S. Multiscale coupling of compliant and rigid walls blood flow models // Int. J. Numer. Meth. Fluids. — 2016. — Vol. 82, No. 12. — P. 799–817.

El Khatib N., Kafi O., Sequeira A., Simakov S., Vassilevski Yu., Volpert V. Mathematical modelling of atherosclerosis // Math. Model. Nat. Phenom. — 2019. — Vol. 14, No. 6. — 603.

Gamilov T., Kopylov P., Simakov S. Computational simulations of fractional flow reserve variability // Numerical Mathematics and Advanced Applications ENUMATH 2015. — 2016. — P. 499–507.

Gamilov T., Liang F., Kopylov P., Kuznetsova N., Rogov A., Simakov S. Computational analysis of hemodynamic indices based on personalized identification of aortic pulse wave velocity by a neural network // Mathematics. — 2023. — Vol. 11, No. 6. — 1358.

Gamilov T., Danilov A., Chomakhidze P., Kopylov P., Simakov S. Computational analysis of hemodynamic indices in multivessel coronary artery disease in the presence of myocardial perfusion dysfunction // Computation. — 2024. — Vol. 12, No. 6. — 110.

Goodfellow I., Bengio Y., Courville A. Deep Learning. — Cambridge, MA: MIT Press, 2016. — 800 p.

Hohri Y., Chung M. M., Kandula V., Kim I., Leb J., Hayashi H., Elmously A., O'Donnell T. F., Patel V., Vedula V., Takayama H. Blood flow assessment technology in aortic surgery: a narrative review // J. Thorac. Dis. — 2024. — Vol. 16, No. 4. — P. 2623–2636.

Iliadis P., Petridis S., Skembris A., Rakopoulos D., Kosmatopoulos E. Physics-informed neural networks for enhanced state estimation in unbalanced distribution power systems // Appl. Sci. — 2025. — Vol. 15. — 7507.

Isaev A., Dobroserdova T., Danilov A., Simakov S. Physically informed deep learning technique for estimating blood flow parameters in four-vessel junction after the fontan procedure // Computation. — 2024. — Vol. 12, No. 3. — 41.

Kasapis C., Gurm H. S. Current approach to the diagnosis and treatment of femoral-popliteal arterial disease. A systematic review // Curr. Cardiol. Rev. — 2009. — Vol. 5, No. 4. — P. 296–311.

Kim H. J., Lee C. M., Choi Y., Chang H., Jung K.-H. Multiscale modeling of posture-dependent cerebrovascular hemodynamics with autoregulatory coupling // Comput. Biol. Med. — 2026. — Vol. 203. — 111502.

Lan H., Updegrove A., Wilson N. M., Maher G. D., Shadden S. C., Marsden A. L. A re-engineered software interface and workflow for the open-source SimVascular cardiovascular modeling package // J. Biomech. Eng. — 2018. — Vol. 140, No. 2. — 0245011.

Liu Z., Liu Y., Yan X., Liu W., Nie H., Guo S., Zhang C. Automatic network structure discovery of physics informed neural networks via knowledge distillation // Nat. Commun. — 2025. — Vol. 16. — 9558.

Ma L., Liu Y., Zhao X., Ren X., Bai F., Ding J., Zhang M., Wang W., Xie J., Zhang H., Zhao Z., Han H. Hemodynamic influence of different pulmonary stenosis degree in Glenn procedure: a numerical study // Adv. Mech. Eng. — 2014. — Vol. 2014. — 72370.

Raissi M., Perdikaris P., Karniadakis G. E. Physics-informed neural networks: A deep learning framework for solving forward and inverse problems involving nonlinear partial differential equations // J. Comput. Phys. — 2019. — Vol. 378. — P. 686–707.

Rasooli R., Pekkan K., Larsen A. I., Hiorth A. Assessment of guidewire-induced deviation in fractional flow reserve: impact of lesion morphology and pressure guidewire malposition // International Journal for Numerical Methods in Biomedical Engineering. — 2025. — Vol. 41, No. 11. — P. e70112.

Sahni O., Carothers C., Shephard M., Jansen K. Strong scaling analysis of a parallel, unstructured, implicit solver and the influence of the operating system interference // Scientific Programming. — 2009. — Vol. 17. — P. 261–274.

Simakov S. S., Gamilov T. M., Liang F., Gognieva D. G., Gappoeva M. K., Kopylov P. Yu. Numerical evaluation of the effectiveness of coronary revascularization // Russian Journal of Numerical Analysis and Mathematical Modelling. — 2021. — Vol. 36, No. 5. — P. 303–312.

Taebi A. Deep learning for computational hemodynamics: A brief review of recent advances // Fluids. — 2022. — Vol. 7, No. 6. — 197.

Tu S., Westra J., Adjedj J., Ding D., Liang F., Xu B., Holm N. R., Reiber J. H. C., Wijns W. Fractional flow reserve in clinical practice: from wire-based invasive measurement to image-based computation // Eur. Heart. J. — 2020. — Vol. 41, No. 34. — P. 3271–3279.

Updegrove A., Wilson N. M., Merkow J., Lan H., Marsden A. L., Shadden S. C. SimVascular: an open source pipeline for cardiovascular simulation // Ann. Biomed. Eng. — 2017. — Vol. 45, No. 3. — P. 525–541.

Vassilevski Yu., Simakov S., Salamatova V., Ivanov Yu., Dobroserdova T. Blood flow simulation in atherosclerotic vascular network using fiber-spring representation of diseased wall // Math. Model. Nat. Phenom. — 2011. — Vol. 6. — P. 333–349.

Ventre J., Fullana J.-M., Lagrée P.-Y., Raimondi F., Boddaert N. Reduced models for computing pressure drop across stenosis // Comput. Methods Biomech. Biomed. Engin. — 2019. — Vol. 22, No. sup1. — P. S119–S120.

Vignon-Clementel I. E., Figueroa C. A., Jansen K. E., Taylor C. A. Outflow boundary conditions for three-dimensional finite element modeling of blood flow and pressure in arteries // Computer Methods in Applied Mechanics and Engineering. — 2006. — Vol. 195, No. 29–32. — P. 3776–3796.

Xia Y., Wang C., Wang Y., Liang F. A computational model-based study on trans-stenotic pressure ratio of carotid artery stenosis and its predictive value for cerebral ischemia // Int. J. Numer. Method. Biomed. Eng. — 2025. — Vol. 41, No. 5. — e70044.

Yan Z., Shang D., Chen R., Liu J., Cai X. C. A computational study of the connection between coronary revascularization and cardio-cerebral hemodynamics // Comput. Methods Programs Biomed. — 2025. — Vol. 263. — 108667.

Young D. F., Tsai F. Y. Flow characteristics in models of arterial stenoses. — I. Steady flow // J. Biomech. — 1973. — Vol. 6, No. 4. — P. 395–410.

Zhang X., Mao B., Che Y., Kang J., Luo M., Qiao A., Liu Y., Anzai H., Ohta M., Guo Y., Li G. Physics-informed neural networks (PINNs) for 4D hemodynamics prediction: An investigation of optimal framework based on vascular morphology // Comput. Biol. Med. — 2023. — Vol. 164. — 107287.

Zimmermann F. M., Mast T. P., Johnson N. P., Everts I., Hennigan B., Berry C., Johnson D. T., De Bruyne B., Fearon W. F., Oldroyd K., Pijls N. H. J., Tonino P. A. L., van 't Veer M. Deep learning for prediction of fractional flow reserve from resting coronary pressure curves // EuroIntervention. — 2021. — Vol. 17, No. 1. — P. 51–58.